Supplement of The Cryosphere, 17, 4511–4533, 2023
https://doi.org/10.5194/tc-17-4511-2023-supplement

The Cryosphere Open Access EGU

Supplement of

Allometric scaling of retrogressive thaw slumps

Jurjen van der Sluijs et al.

Correspondence to: Jurjen van der Sluijs (jurjen_vandersluijs@gov.nt.ca)

Supplemental materials to Van der Sluijs et al., *Allometric scaling of retrogressive thaw slumps*

S1: Methods overview

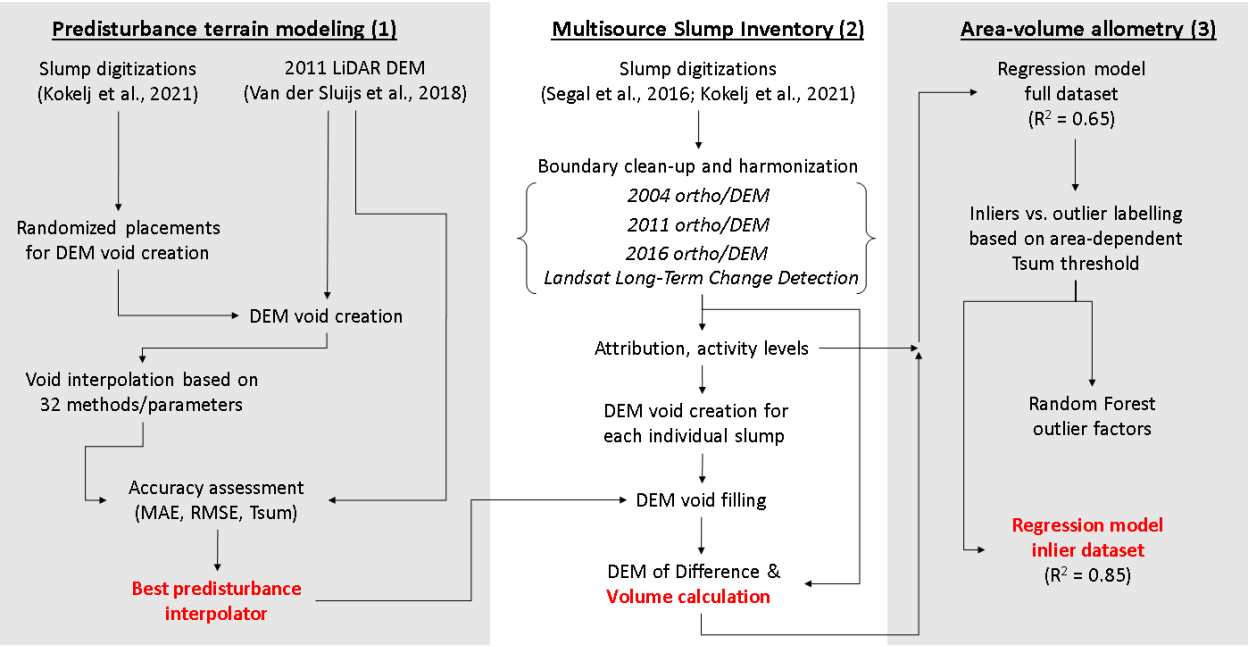

Figure S1: Flowchart of methods to achieve study objectives.

S2: Additional elevation dataset descriptions

At the smallest geographic extent and within the Inuvik-to-Tuktoyaktuk (ITH) and Dempster Highway (DH) corridors, airborne stereo-photogrammetry and LiDAR surveys were acquired in 2011. For detailed descriptions of acquisition and data processing readers are referred to Van der Sluijs et al., (2018).

At a larger geographic extent airborne stereo-photogrammetry from 2004 was used to derive 1-m contour lines which were interpolated to 3-m hydrologically correct DEMs using ArcGIS 10.6.1 "Topo-to-Raster" tool (based on ANUDEM). The 2004 DEM tiles were compared to ITH and DH LiDAR elevations based on 10,000 samples per 10 km^2 tile where the datasets overlapped. This resulted in a R^2 range between 0.98-0.99 and Root Mean Square Differences of 1.28-1.46 m (i.e., sub-pixel vertical uncertainties without correcting for vertical datum differences).

Finally, seamless mosaics of the pan-Arctic data product ArcticDEM were used to enable work at the largest geographical extent possible. The DEM has been developed by the Polar Geospatial Center, based on very high stereo-satellite imagery, and the most recent product at the time of digitization (version 7) has undergone additional post-processing steps to ensure data consistency among tiles. The mosaiced dataset has a median acquisition year of 2016 for either study region (based on n=66 and 132 strips for PP and APTC, respectively). The mosaic tiles were the best available ArcticDEM data at the time of digitization, yet sometimes are affected by NoData holes due to cloud cover or lack of stereo-coverage. The imagery used for the regional scale ortho-mosaic was sourced from the ESRI World Imagery Layer. Metadata for this base imagery indicated a median acquisition year of 2017 for the blended tiles (n = 39 and 20 for ATPC and PP, respectively). The ArcticDEM mosaics were compared to ITH and DH LiDAR elevations based on 19,762 random sampling locations (minimum nearest neighbor distance = 200 m) located outside of water bodies, slump disturbances, and known temporal changes or noise areas (n= 16,369 for APTC, n = 3,393 for PP). Mean biases introduced due to vertical datum differences and other sources were removed prior to LiDAR comparisons (+5.30 m for APTC, -2.14 m). This resulted in a $R^2 > 0.99$ for either study area and RMSDs of 1.23 m and 1.42 m for APTC and PP, respectively.

Table S1: Overview of DEM datasets

DEM	Year	Technology	Spatial Resolution	Hor./ Vert. accuracy	References
MVAP [1]	2004	Airborne stereo-photogrammetry	3 m	± 1.5 m	NWT Centre for Geomatics (2008). Ortho-mosaic previously used by Lantz and Kokelj (2008) and Segal et al., 2016)
LiDAR	2011	LiDAR	1 m	± < 0.2 m	Van der Sluijs et al., (2018)
ArcticDEM [2]	2016 (circa)	Satellite stereo-photogrammetry	2 m	± 1.2 to 1.4 m	Porter et al., (2018)

[1] Mackenzie Valley Airphoto Project (MVAP) of Indian and Northern Affairs Canada, now Government of Northwest Territories. The MVAP dataset in this study represents a small subset of the entire dataset hosted by the NWT Centre for Geomatics.

[2] DEM(s) were created from DigitalGlobe, Inc., imagery and funded under National Science Foundation awards 1043681, 1559691, and 1542736.

S3: Interpolation methods

Table S2: Overview of interpolation methods and their performance to reconstruct pre-erosional terrain.

ID	Suite	Main Parameter	Abr.	RMSD (m)			
				Median	IQR	90th %	95th%
1	IDW	Power of 0.5 [1]	IDW05	0.82	1.00	2.80	4.04
2	IDW	Power of 1.0 [1]	IDW10	0.82	1.00	2.80	4.04
3	IDW	Power of 1.5 [1]	IDW15	0.82	1.00	2.80	4.04
4	IDW	Power of 2.0 [1]	IDW20	0.82	1.00	2.80	4.04
	IDW			0.82	1.00	2.80	4.04
5	**TR**	**Linear**	**LIN**	**0.26**	**0.39**	**1.02**	**1.42**
6	**TR**	**Natural Neighbour**	**NN**	**0.28**	**0.38**	**1.03**	**1.40**
	TR			**0.27**	**0.38**	**1.03**	**1.42**
7	RSL	Weight of 0.000 [2]	RSL0	0.55	0.73	2.16	3.30
8	RSL	Weight of 0.001 [2]	RSL0001	0.55	0.71	2.13	2.98
9	RSL	Weight of 0.005 [2]	RSL0005	0.57	0.74	2.17	3.14
10	RSL	Weight of 0.01 [2]	RSL001	0.60	0.77	2.28	3.32
11	RSL	Weight of 0.05 [2]	RSL005	0.76	0.99	3.07	4.44
12	RSL	Weight of 0.10 [2]	RSL01	0.89	1.13	3.31	4.67
	RSL			0.64	0.86	2.52	3.61
13	RSH	Weight of 0.33 [2]	RSH03	1.21	1.49	4.56	6.37
14	RSH	Weight of 0.50 [2]	RSH05	1.36	1.69	5.06	7.19
15	RSH	Weight of 1.00 [2]	RSH1	1.64	2.09	6.21	8.83
16	RSH	Weight of 5.00 [2]	RSH5	2.24	3.08	8.85	12.65
	RSH			1.55	2.10	6.15	8.82
17	ST	Weight of 0.0 [3]	ST0	66.49	200.62	646.19	1332.49
18	ST	Weight of 1.0 [3]	ST1	0.72	0.98	2.89	4.06
19	ST	Weight of 3.0 [3]	ST3	0.75	1.00	2.90	4.07
20	ST	Weight of 5.0 [3]	ST5	0.76	1.01	2.91	4.08
21	ST	Weight of 7.0 [3]	ST7	0.77	1.01	2.91	4.08
22	ST	Weight of 9.0 [3]	ST9	0.77	1.00	2.91	4.08
23	ST	Weight of 10.0 [3]	ST10	0.78	1.01	2.91	4.08
	ST			0.93	2.03	26.90	136.30
24	EBK [4, 5]	No transform, Power	EBK-POW	0.51	0.73	2.13	2.98
25	EBK	No transform, Linear	EBK-LIN	0.71	0.95	2.70	3.93
26	EBK	No transform, Thin Plate Spline	EBK-TPS	0.55	0.80	2.49	3.47
	EBK			0.59	0.84	2.44	3.41
27	EBK-EMP	Empirical transform, Exponential	EBK-EXP	0.84	1.09	2.97	4.27
28	EBK-EMP	Empirical transform, Whittle	EBK-WHIT	0.81	1.08	2.97	4.28
29	EBK-EMP	Empirical transform, K-Bessel	EBK-KBES	0.79	1.12	2.98	4.30
	EBK-EMP			0.81	1.09	2.98	4.28
30	EBK-EMPD	Empirical transform, Exponential detrended	EBK-EXPD	0.38	0.57	1.71	2.46
31	EBK-EMPD	Empirical transform, Whittle detrended	EBK-WHITD	0.38	0.60	1.75	2.50
32	EBK-EMPD	Empirical transform, K-Bessel detrended	EBK-KBESD	0.38	0.60	1.77	2.61
	EBK-EMPD			0.38	0.59	1.75	2.54

[1] Power describes the exponent of distance parameter, which controls the significance of surrounding points on the interpolated value. A higher power results in less influence from distant points.
[2] Weight is the square of the parameter referred to as tau (t). Higher values produce smoother surfaces (typical range: 0 to 0.5).
[3] Weight is the square of the parameter referred to as phi (Φ). Higher values produce coarser surfaces and more closely conform to input points (typical range: 0 to 10).
[4] Empirical Bayesian Kriging (EBK) was selected as an alternative over other kriging methods (e.g., ordinary kriging) to overcome challenges in the proper manual selection of the type of theoretical variogram model and semivariogram parameters.
[5] EBK offers both settings for data transformation (*none* or Multiplicative Skewing transformation with *Empirical* base function) and various *semivariogram* models.

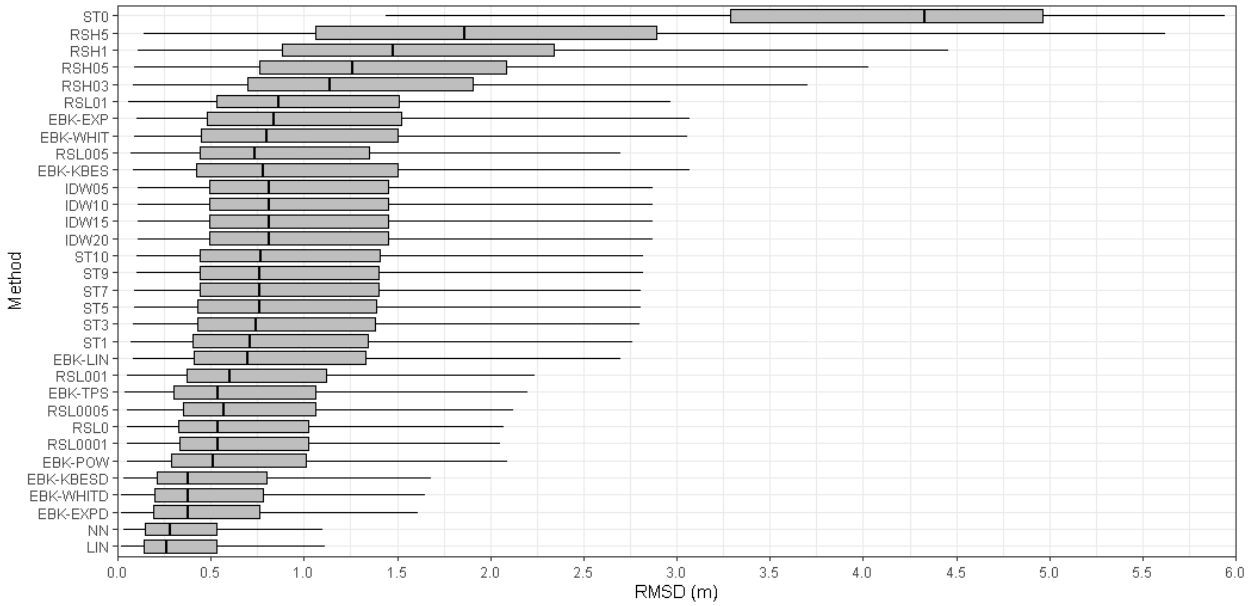

Figure S2: Boxplot of deviations between actual and modelled elevation (expressed as Root Mean Square Difference; RMSD) for each interpolation method. Due to outliers in ST with a weight of zero (ST0) the X-axis was limited to 6 m (representing triple the upper quartile (75th percentile) of the entire dataset), removing 1,668 model observations from presentation.

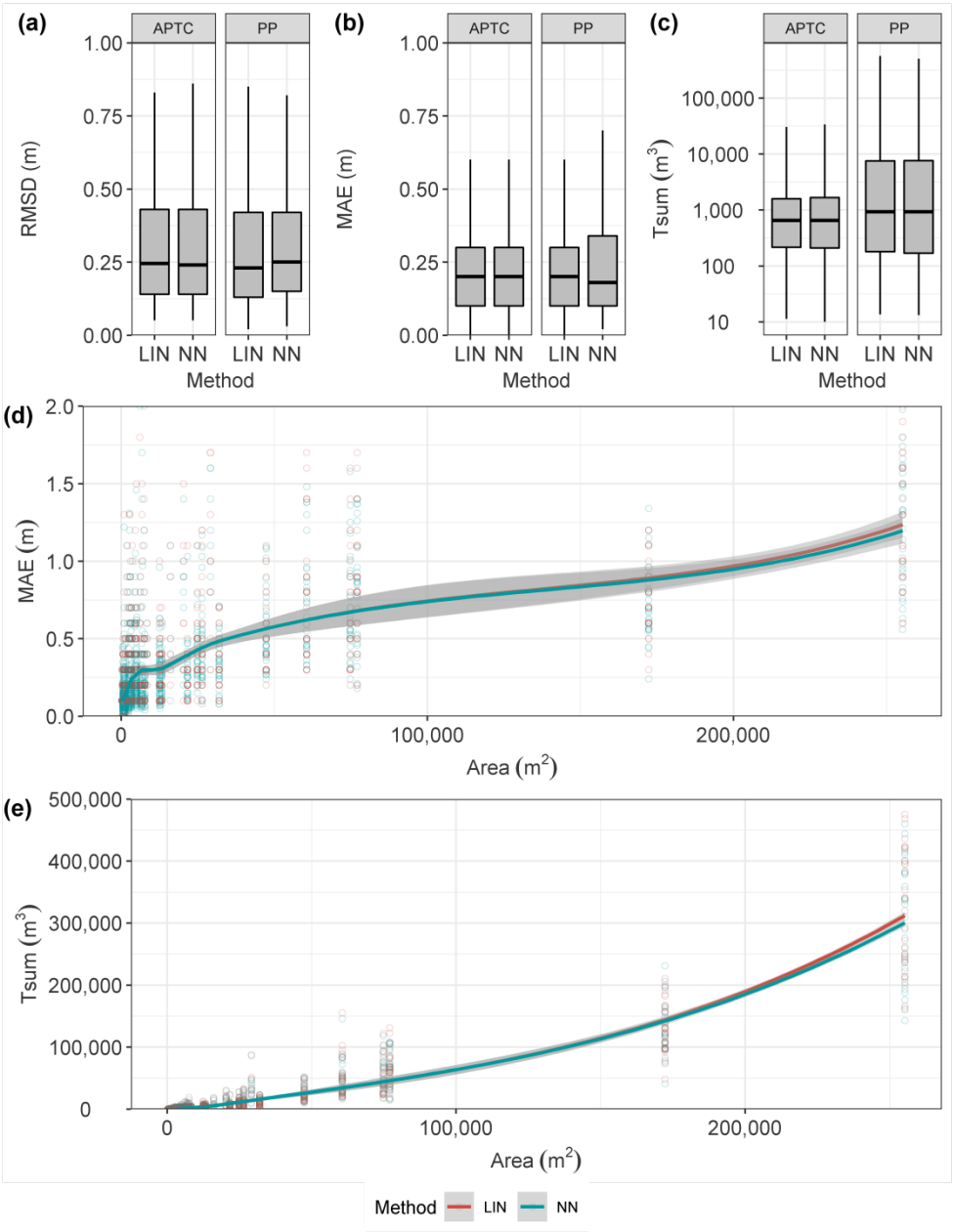

Figure S3: Deviations between actual and modelled elevation for linear (LIN) and natural neighbour interpolation (NN), expressed as boxplots based on Root Mean Square Difference (a), Mean Absolute Error (b) and summed topographic difference (c) along with two scatterplots between void surface area and MAE (d) and T_{sum} (e), respectively, with loess smoothing lines to highlight the degree to which the interpolation methods exhibit area-dependent uncertainty.

S4: Python code

Python code developed for this work (DEM_PredisturbanceGeneration_AreaVolumeCalc_Batch_NN_Py3.py) is provided as-is without warranties or assurances.

Dependencies:

- Developed/tested using ESRI ArcGIS Pro v2.7 to v2.9 with ArcPy, Spatial Analyst or 3D Analyst
- Developed/tested using Python 3.7.11 [MSC v.1927 64 bit (AMD64)] on win32

Inputs:

- Shapefile(s) of slump delineations
- Digital elevation model (Geotif)

Outputs:

- Database file (.BDF) of slump structural estimates, including volume (SUM attribute) and average depth-of-thaw estimates (MEAN and MEDIAN attributes).

Considerations:

- Shapefile must have a "UniqueID" attribute.
- Shapefile is allowed to have overlapping polygons, which normally provide erroneous *ArcGIS Zonal Statistics as Table* results as polygons are normally rasterized before raster statistics are generated. In the provided Python code features are processed iteratively in batch mode, thus this limitation has been overcome.
- If the spatial resolution of the input DEM is not 1 m, a multiplication is required in order to derive volumes in cubic metres. For example, for the 2 m resolution ArcticDEM this factor is 2 x 2 = 4. For a 3 m DEM such as MVAP this factor is 3 x 3 = 9. This functionality is not included in the code and needs to be applied afterwards.

S5: Slump volumes used for allometry

Slump volume estimates generated for this analysis are stored in the file "MSI_2022_10_Volumes_Outlierclass.shp" available in the supplement. Allometry was established based on the "Area_m" attribute and the "Volume_m" attribute. To access landscape descriptors, two-dimensional geometry estimates, three-dimensional hypsometry estimates, and activity ratings, readers are referred to the Van der Sluijs and Kokelj (2023) Open Report. The two shapefiles can be joined based on the "FeatID" attribute.

Table S3: List of attributes of slump volume shapefile.

Attribute	Description
Area_m	Area in meters squared, calculated based on shapefile (NAD83 CSRS UTM Zone 8N)
Easting	Easting of slump centre coordinate (NAD83 CSRS UTM Zone 8)
Northing	Northing of slump centre coordinate (NAD83 CSRS UTM Zone 8)
Datasource	MVAP, LiDAR (ALS) or ArcticDEM (AD)
Year	Year of observation
UniqueID	Sequential number of each landslide entry in the database, per region
FeatID	Sequential number of each landslide entry in the database
Region	APTC or PP
COUNT [1]	Sampled pixels in scar zone
DODMIN [1]	Largest decreasing elevation change, sampling all pixels in scar zone
DODMAX [1]	Largest increasing elevation change, sampling all pixels in scar zone
DODRANGE [1]	Range of elevation changes, sampling all pixels in scar zone
DODMEAN [1]	Mean elevation change, sampling all pixels in scar zone
DODSTD [1]	Standard deviation of elevation change, sampling all pixels in scar zone
DODSUM [1]	Sum of all positive and negative elevation changes, sampling all pixels in shapefile
DODMEDIAN [1]	Median elevation change, sampling all pixels in scar zone
DODf	Multiplier to derive volumes in cubic metres, in case input DEM does not have 1 m spatial resolution
Volume_m	Product of DODSUM and DODf, representing scar zone volumes in cubic metres.
nn_fit	*Tsum* uncertainty threshold defined by relationship shown in Fig. 5b and Eq. 2.
DODcls	Inlier versus outlier classification, based on nn_fit threshold. If DODmean was positive or if Volume_m was smaller than nn_fit the assigned class was 0 (outlier). If not, the assigned class was 1 (inlier).

[1] Derived using Python script (S4), based on Zonal Statistics as Table tool in ArcGIS Pro.

References

Kokelj, S. V., Kokoszka, J., van der Sluijs, J., Rudy, A. C. A., Tunnicliffe, J., Shakil, S., Tank, S. E., and Zolkos, S.: Thaw-driven mass wasting couples slopes with downstream systems, and effects propagate through Arctic drainage networks, The Cryosphere, 15, 3059–3081, https://doi.org/10.5194/tc-15-3059-2021, 2021.

Lantz, T. C. and Kokelj, S. V.: Increasing rates of retrogressive thaw slump activity in the Mackenzie Delta region, N.W.T., Canada, Geophysical Research Letters, 35, https://doi.org/10.1029/2007GL032433, 2008.

NWT Centre for Geomatics.: MVAP Mosaic Combined [dataset]. Yellowknife, NT, Canada. https://www.image.geomatics.gov.nt.ca/arcgis/rest/services/Mosaics/MVAP_Mosaic_Combined_LCC/MapServer

NWT Centre for Geomatics.: Landsat Long-term Change Detection [dataset]. Yellowknife, NT, Canada, 2021. https://www.image.geomatics.gov.nt.ca/arcgis/rest/services/Mosaics/LongTermChangeDetection_TasseledCapResult/ImageServer

Porter, C., Morin, P., Howat, I., Noh, M.-J., Bates, B., Peterman, K., Keesey, S., Schlenk, M., Gardiner, J., Tomko, K., Willis, M., Kelleher, C., Cloutier, M., Husby, E., Foga, S., Nakamura, H., Platson, M., Wethington, M., Williamson, C., Bauer, G., Enos, J., Arnold, G., Kramer, W., Becker, P., Doshi, A., D'Souza, C., Cummens, P., Laurier, F., and Bojesen, M.: ArcticDEM, 2018.

Segal, R. A., Lantz, T. C., and Kokelj, S. V.: Acceleration of thaw slump activity in glaciated landscapes of the Western Canadian Arctic, Environmental Research Letters, 11, 034025, 2016.

Van der Sluijs, J., Kokelj, S. V., Fraser, R. H., Tunnicliffe, J., and Lacelle, D.: Permafrost Terrain Dynamics and Infrastructure Impacts Revealed by UAV Photogrammetry and Thermal Imaging, Remote Sensing, 10, 1734, 2018.

Van der Sluijs, J. and Kokelj, S. V.: High-resolution inventory of retrogressive thaw slump affected slopes using high spatial resolution Digital Elevation models and imagery, Peel Plateau and Anderson Plain – Tuktoyaktuk Coastlands, Northwest Territories, Northwest Territories Geological Survey, https://doi.org/10.46887/2023-013, 2023.